REVIEW OF SCIENTIFIC INSTRUMENTS **89**, 123706 (2018)

Antiferromagnetic MnNi tips for spin-polarized scanning probe microscopy

P. R. Forrester,[1,2] T. Bilgeri,[1] F. Patthey,[1] H. Brune,[1,a)] and F. D. Natterer[1,2,a)]
[1]*Institute of Physics, École Polytechnique Fédérale de Lausanne, CH-1015 Lausanne, Switzerland*
[2]*Physik-Institut, University of Zurich, Winterthurerstrasse 190, CH-8057 Zurich, Switzerland*

(Received 1 June 2018; accepted 28 November 2018; published online 18 December 2018)

Spin-polarized scanning tunneling microscopy (SP-STM) measures magnetoresistance with atomic resolution. While various methods for achieving SP probes have been developed, each is limited with respect to fabrication, performance, and operating conditions. In this study, we present the fabrication and use of SP-STM tips made from commercially available antiferromagnetic $Mn_{88}Ni_{12}$ foils. The tips are intrinsically SP, which is attractive for exploring magnetic phenomena in the zero field limit. The tip material is relatively ductile, is straightforward to etch, and has a Néel temperature exceeding 300 K. We benchmark the topographic and spectroscopic performance of our tips and demonstrate their spin sensitivity by measuring the two-state switching of holmium single atom magnets on MgO/Ag(100). *Published by AIP Publishing.* https://doi.org/10.1063/1.5042530

I. INTRODUCTION

Spin-polarized scanning tunneling microscopy (SP-STM)[1–4] is an essential technique for investigating magnetism at the microscopic level, ranging from the study of magnetic skyrmions,[5,6] single atoms, and molecules[7–12] to the observation of Majorana modes,[13,14] spin filter measurements,[15,16] and electron spin resonance.[17] Moreover, SP-STM should facilitate further understanding of topological states in graphene systems,[18,19] topological insulators,[20] and transition metal dichalcogenides.[21] Spin-polarized STM demands that tips have a stable SP density of states (DOS) at the tunneling apex, in addition to being sufficiently sharp to achieve atomic resolution and spectroscopically stable over a large bias range for scanning tunneling spectroscopy (STS). An ideal SP-STM tip would also have a directionally adjustable magnetization component for in-plane and out-of-plane sensitivity. Although past efforts using bulk ferromagnets as tips and coating nonmagnetic tips with magnetic thin films yielded high spin contrast, they exhibited sizeable stray fields.[22–28] The functionalization of nonmagnetic tips with atoms or clusters of magnetic atoms also yields spin contrast but is tedious, is time consuming, and generally requires an external magnetic field to orient the paramagnetic tip-moment.[29] Tips fabricated from antiferromagnetic bulk materials, on the other hand, are intrinsically spin-polarized and tend to minimize the stray field. A large body of work focuses on chromium as a tip material,[30–33] but the brittleness of Cr renders tip preparation difficult and motivates the search for alternative materials. Antiferromagnetic $Mn_{50}Ni_{50}$ has also been reported as a SP-STM tip material, but synthesis of this alloy requires specialized arc-melting.[34] The antiferromagnetic $Mn_{88}Ni_{12}$ alloy is an attractive alternative for SP-STM as it contains a higher concentration of Mn, which is responsible for the spin sensitivity of the material.[35–37] This alloy is commercially available and has a Néel temperature greater than 300 K,[35] probably making the tips suitable for room temperature SP-STM. We find that tips made from foils of $Mn_{88}Ni_{12}$ yield high spin contrast, are easy to etch electrochemically, are robust during handling, and perform equally well in topographic and spectroscopic modes as our previously used W and Pt/Ir tips.

II. TIP FABRICATION

We fabricate $Mn_{88}Ni_{12}$ tips via a conventional loop etching method[38] in a homebuilt tip etching station shown in Fig. 1(a). A commercially available 0.25 mm thick $Mn_{88}Ni_{12}$ foil (Goodfellow) is cut into square rods via electrical discharge machining. We find that this method yields superior rods compared to laser cutting. The latter typically results in irregular rod geometries that lead to undesired anisotropic etching and thus blunt tips, as also suggested by Murphy *et al.*[34] The cut rod is lowered into a meniscus of 13% aqueous hydrochloric acid (HCl), supported by an inert platinum ring. The rod is held at +10 V relative to the Pt ring, facilitating electrochemical etching of the region in contact with the solution. The gaseous products of the reaction frequently break the meniscus, requiring repeated rewetting of the loop. This does not appear to affect the tip quality as the meniscus re-forms around the etched area due to its high surface area. After about 3 min, the eroded area can no longer support the weight of the lower portion and breaks. This part lands on a bed of shaving cream that prevents damage to the atomically sharp candidate tip. The voltage is then immediately removed to slow the electrochemical etching of the top part. Since both parts of the etched rods are tip candidates, we rinse them in deionized water, acetone, and isopropanol and blow them dry using dry-nitrogen. We notice chlorine salt formation and further etching without the previous steps, possibly due to the reactivity of the etchant even without applied bias. We examine the candidate tips under a stereomicroscope. Typically, 20% of these tips are judged as sufficiently sharp to warrant further investigation with scanning electron microscopy (SEM).

a)Authors to whom correspondence should be addressed: fabian.natterer@uzh.ch and harald.brune@epfl.ch

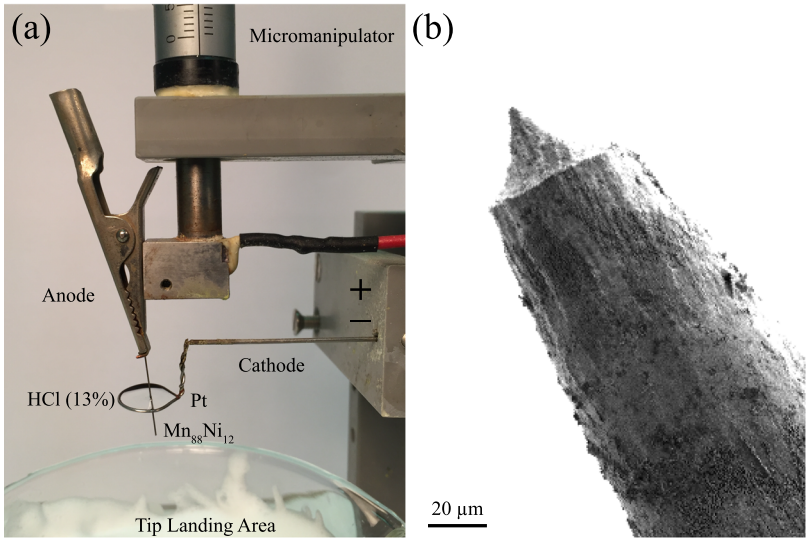

FIG. 1. (a) Photograph of the tip etching station. A $Mn_{88}Ni_{12}$ rod is held at a positive bias relative to a meniscus of 13% HCl suspended by an inert platinum ring. When the electrochemically eroded section can no longer support the weight of the lower segment of the rod, it breaks, and the lower segment lands on a mousse of shaving cream, preserving the sharp tip apex. (b) SEM micrograph of a representative $Mn_{88}Ni_{12}$ tip, imaged at a beam energy of 1.5 keV.

Figure 1(b) shows an SEM micrograph of such a tip. The best tips are crimped onto a homemade tip holder, transferred into our ultra-high vacuum chamber, and bombarded with a 1 kV beam of Ar^+ ions at an angle of 30° off the tip axis for 30 min at an Ar partial pressure of 5×10^{-5} mbar. This treatment removes residual contamination from etching, including Cl salts, hydrocarbons, and oxides.

III. SCANNING TUNNELING MICROSCOPY

A. Scanning tunneling microscopy/spectroscopy

We evaluate the performance of the $Mn_{88}Ni_{12}$ tips on the model systems of MgO/Ag(100) and TiH/MgO by reproducing topographic and spectroscopic characteristics detailed in previous studies.[39–42] Figure 2(a) shows a large-scale topographic

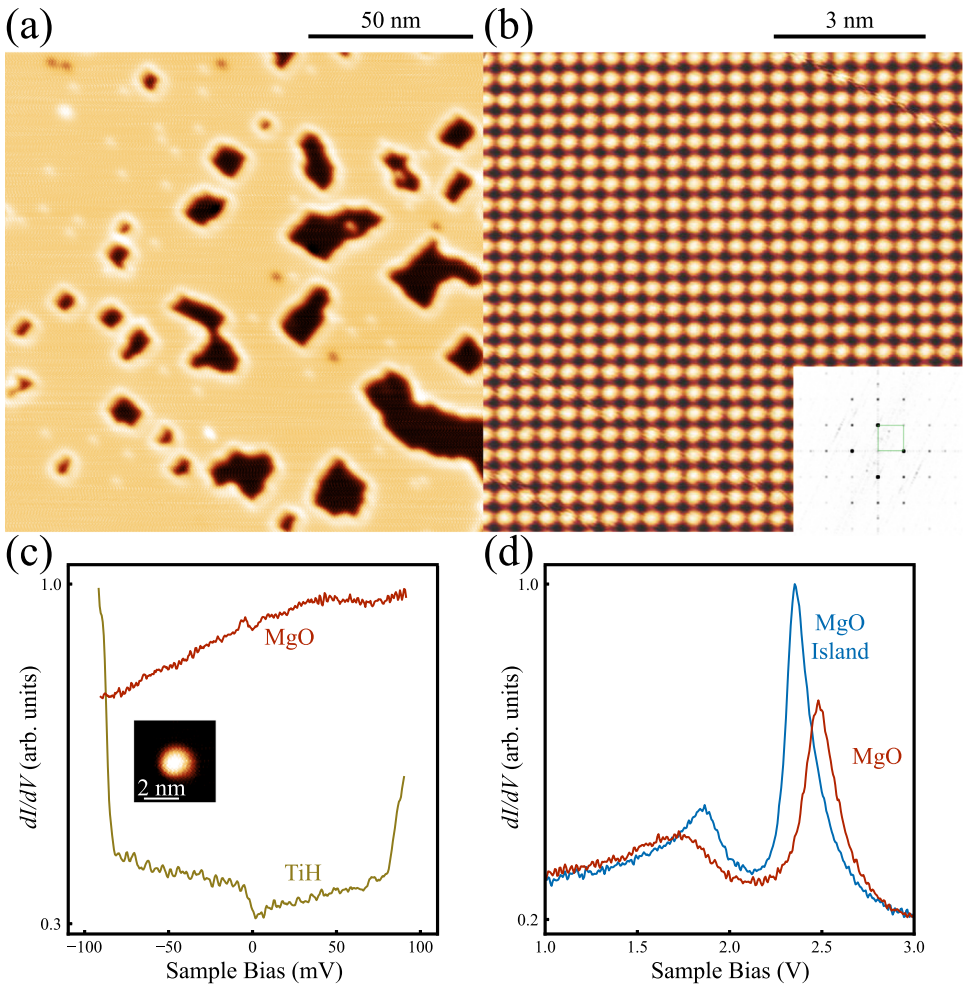

FIG. 2. (a) STM topographic image of MgO/Ag(100). Dark regions correspond to MgO islands (V = 1 V, I = 100 pA). (b) Atomically resolved STM image of MgO in (a) (V = −20 mV, I = 10 nA). Inset: 2D fast Fourier transform of (b) with the reciprocal unit cell outlined (green). (c) dI/dV point spectra of TiH (gold) and MgO (red) (V = −100 mV, I = 200 pA for TiH and V = −100 mV, I = 500 pA for MgO). Inset: STM image of a TiH (V = −100 mV, I = 100 pA). (d) Field emission resonance spectra of MgO (red) and island (blue) (V = 1 V, I = 100 pA).

STM image of MgO/Ag(100) measured with our $Mn_{88}Ni_{12}$ tip. We observe a smooth MgO layer and the nucleation of additional MgO islands, imaged here as depressions due to their lower DOS up to the tunneling bias of 1 V. Our tip also resolves sharp atomic steps and isolated point defects over the large scan range in agreement with previous work.[40] The tips routinely achieve atomic resolution, as demonstrated in Fig. 2(b). The (1 × 1) oxygen sublattice of MgO is clearly reproduced as emphasized by the 2D FFT inset in Fig. 2(b).

We benchmark the spectroscopic performance of our $Mn_{88}Ni_{12}$ tips via STS. The *dI*/*dV* spectra recorded on MgO (red) and a hydrogenated Ti adatom (TiH, gold)[42] are shown in Fig. 2(c). The essentially featureless MgO spectrum agrees with earlier results using non-SP tips[41] and demonstrates the smooth tip DOS. Our tip is thus sensitive to sample details and reproduces the large conductance steps of TiH at ~80 mV known from previous work.[42] In view of the well-behaved spectroscopy at low voltages, we examine the tip's performance at higher biases via field-emission resonance (FER) spectroscopy. Figure 2(d) shows a FER measurement of the MgO (red) and an MgO island (blue) in Fig. 2(a). We see an energetic downshift in the higher peak and an upshift in the lower peak with the addition of an MgO layer, in agreement with previous studies.[40,43]

B. Spin-polarized scanning tunneling microscopy

To test our $Mn_{88}Ni_{12}$ tips' spin-polarization, we dose holmium atoms [inset of Fig. 3(b)] in addition to TiH onto MgO. Holmium is known to have a stable out-of-plane magnetization on the oxygen adsorption site.[8,44] It exhibits tunnel magnetoresistance (TMR) when measured with a SP-tip through which the magnetic state can be read non-destructively for tunnel voltages $V \leq 73$ mV.[8] Furthermore, the Ho magnetization may be switched between the *up* and *down* orientations for voltages above this threshold, resulting in conductance changes when measured with an out-of-plane sensitive SP tip.[8] We exploit this phenomenon to prove the spin-sensitivity of our tip. The schematics in Figs. 3(a) and 3(b) illustrate the two magnetic states of holmium, up and down, and the out-of-plane projected SP-DOS of the tip. When the majority spin occupation of the SP-DOS of the tip coincides with that of the Ho, the resistance is small (large current). Conversely, the resistance is large (small current) when the majority occupation of the SP-DOS of the tip coincides with the minority occupation of the Ho atom.

Figure 3(c) shows voltage dependent tunnel current time-traces, measured on MgO and Ho using our SP-tip. The current on the MgO substrate is constant, as expected. We also measure constant current on the Ho atom for a bias voltage of 60 mV. However, at higher voltages (80, 90, and 110 mV), we observe an accelerating two-state switching. In agreement with the aforementioned threshold voltage for magnetic switching,[8] the current trace at 60 mV simply probes one of the two magnetic Ho states. The two-state switching encountered for bias voltages above the switching threshold corresponds to the magnetization reversal of the Ho atom between its up and down states,[8] manifested by a change in the conductance between the two configurations. We observe an average effective spin-polarization of the junction[1] of (6.2 ± 0.1)% and a monotonically increasing switching rate with bias, both in agreement with previous measurements.[8,9] The observed two-state switching of Ho, increase in the switching rate with increased bias, and stability of the Ho state below the threshold voltage unambiguously prove the magnetic sensitivity of our $Mn_{88}Ni_{12}$ tip in the out-of-plane direction.

Note that some microtip configurations yield no magnetic sensitivity to the Ho switching, but applying voltage pulses in the range of 1–10 V reliably yields SP microtips with out-of-plane contrast. We attribute this to two phenomena: (1) The magnetic moment of nickel atoms is quenched in the $Mn_{88}Ni_{12}$ bulk;[45] thus, a Ni terminated tip may not show SP, and (2) the magnetic moment of a Mn terminated tip might be too oblique with respect to that of our Ho test atom, thus leading to a reduced spin contrast in the out of-plane-direction that is insufficient to resolve magnetic switching related conductance changes. The orientation of the apex grain of the tip may be responsible for this. For the latter situation, we would obtain in-plane sensitivity instead, potentially

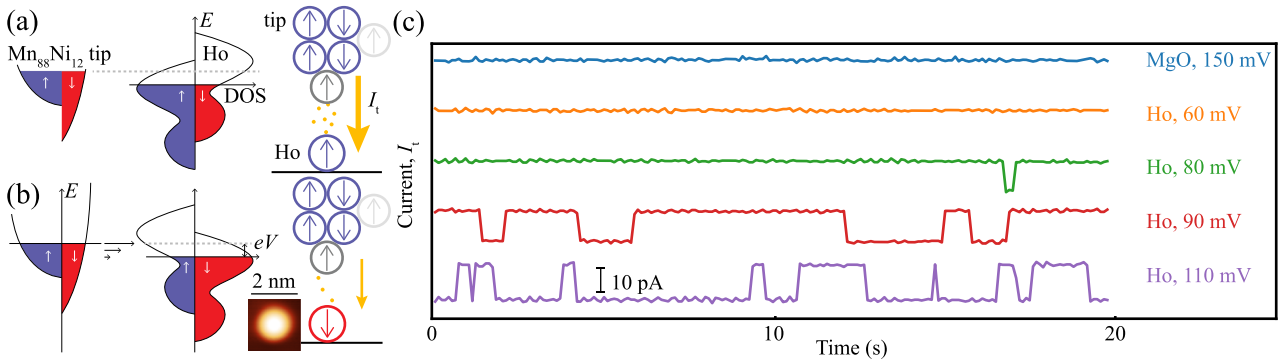

FIG. 3. (a) Tunneling schematics showing larger current for the commensurate tip and Ho majority and minority SP-DOS projected along the out-of-plane direction and (b) smaller current for incommensurate SP-DOS. Inset: STM image of a holmium single atom magnet on MgO/Ag(100) ($V = -50$ mV, $I = 100$ pA). The semitransparent gray atom shows an in-plane SP-tip configuration. (c) Tunneling current-time trace measured on MgO (blue) at 150 mV and on Ho at increasing biases from 60 mV (yellow), to 110 mV (purple) at a nominal set-point current of 100 pA in open *Z*-feedback. The two-state switching of Ho reflects a magnetization reversal of the Ho moment and occurs above a switching threshold of 73 mV. Below this threshold, the orientation of the Ho moment is stable and no switching is observed.

allowing us to *in situ* reconfigure a $Mn_{88}Ni_{12}$ tip for in-plane and out-of-plane measurements by voltage pulsing. Accordingly, our SP-tips show a conductance asymmetry on TiH on MgO around zero bias [Fig. 2(c)], which has been attributed to spin-polarization in the direction of the effective field and that is absent for non-SP tips.[42] The observation of this asymmetry for tips that show negligible TMR on Ho suggests an in-plane spin-sensitivity. The tip curating procedure typically leads to irreversible modifications of the tip apex and the surrounding surface regions, requiring the lateral repositioning of the tip in a new surface spot. This tip-treatment appears to be more reliable for $Mn_{88}Ni_{12}$ than for Cr tips, which inspired our preferential usage of the former.

The tip stray field is dominated by the apex atom, as inferred from a model calculation using a cubic lattice (a = 3.67 Å) and magnetic moments of bulk MnNi[35–37] via the magnetic dipole-dipole interaction. In fact, a Hall measurement of an unetched rod of $Mn_{88}Ni_{12}$ shows no macroscopic field, as expected for a bulk antiferromagnet. We estimate a magnetic dipole stray field of ∼14 mT along the surface normal for the measurement conditions in Fig. 3(c), assuming a tip moment of 2 μ_B[35] at a distance of 6.5 Å between the centers of tip apex atom and the Ho adatom (∼2.5 Å away from point-contact) and the magnetic tip structure sketched in Figs. 3(a) and 3(b). Note that the tip stray field for an in-plane oriented apex atom would be below 10 mT [faded gray atom in Figs. 3(a) and 3(b)]. Due to the poor overlap between the 4*f* and *d* electron-wavefunctions, we do not consider exchange interactions.[42]

IV. SUMMARY AND OUTLOOK

We outlined the fabrication of SP-STM tips from a commercially available $Mn_{88}Ni_{12}$ foil using one step HCl etching. We examined representative candidate tips with SEM, showing the necessary mesoscopic sharpness for STM studies. With these $Mn_{88}Ni_{12}$ tips, we atomically resolve MgO/Ag(100) and reproduce the known spectroscopic features of MgO and TiH. We proved the out-of-plane spin sensitivity by measuring the two state switching of Ho single atom magnets and described tip curation via voltage pulses for reproducibly recovering such spin contrast.

Tips made from $Mn_{88}Ni_{12}$ are promising for magnetic scanning probe experiments. Our work positively identifies $Mn_{88}Ni_{12}$ tips as a powerful, straightforward, and accessible alternative probe material for scanning probe microscopy (SPM) that should enable the advanced study of magnetic phenomena in the absence of an applied magnetic field. These tips provide an avenue for examining magnetic phenomena at near zero effective fields, such as observing Majorana particles, discovering topologically protected states at interfaces, and reading and writing magnetic systems. Furthermore, the relative ease with which $Mn_{88}Ni_{12}$ can be machined to small form factors is encouraging for more involved SPM techniques, such as magnetic force microscopy, where bulkier tips would lead to a prohibitive reduction in the cantilever quality factor. We expect that room temperature SP-SPM studies are possible due to a Néel temperature of more than 300 K.[35]

V. EXPERIMENTAL DETAILS

All measurements are performed in a homebuilt STM[46] at a base pressure below 1×10^{-10} mbar and at a temperature of 4.7 K. The Ag(100) surface is cleaned via alternating cycles of Ar^+ bombardment (∼1 $\mu A/cm^2$) and annealing at 800 K. We grow MgO by dosing Mg from a Knudsen cell evaporator in an O_2 atmosphere of 1×10^{-6} mbar onto the Ag(100) crystal held at 823 K at a rate of ∼0.2 monolayers per minute. Titanium and Ho atoms are deposited from an e-beam evaporator onto the cooled ($T < 10$ K) sample in the STM position. The Ti adatoms become hydrogenated from the residual gas and form TiH.[42,47] All spectroscopic measurements are taken using a lock-in technique with f_{mod} = 397 Hz and V_{mod} = 2 mV_{pp} except for the field emission resonances of MgO, which are measured with f_{mod} = 1397 Hz and V_{mod} = 10 mV_{pp} with Z-feedback engaged. The current-time traces in Fig. 3(c) are measured with open Z-feedback at a nominal current setpoint of I = 100 pA and at the voltages indicated in Fig. 3(c). We subtract a linear background from the current-time traces to account for drift in the tunnel junction. The averaging time for each current data point is 20 ms. All measurements are performed without applied magnetic field. We recommend following standard safety practice as described by OSHA and to place the etching station in a fume hood or well-ventilated area when carrying out tip etching.

SUPPLEMENTARY MATERIAL

See supplementary material for discussion on the orientation of the spin sensitivity of $Mn_{88}Ni_{12}$ tips, the tip-originating magnetic stray field calculations, and contamination from tip etching.

ACKNOWLEDGMENTS

We thank the mechanical workshop of the EPFL Institute of Physics for expert technical assistance and the *Centre Interdisciplinaire de Microscopie Électronique* (CIME) for SEM characterization. P.R.F. appreciates support from the Fulbright U.S. Student Program. F.D.N., P.R.F., and T.B. thank the Swiss National Science Foundation for support under Project Nos. PZ00P2_167965, 200020_176932, and PP00P2_176866.

[1] R. Wiesendanger, Rev. Mod. Phys. **81**, 1495 (2009).
[2] M. Julliere, Phys. Lett. A **54**, 225 (1975).
[3] S. Phark and D. Sander, Nano Convergence **4**(8), 1 (2017).
[4] W. Wulfhekel and J. Kirschner, Annu. Rev. Mater. Res. **37**, 69 (2007).
[5] N. Romming, C. Hanneken, M. Menzel, J. E. Bickel, B. Wolter, K. von Bergmann, A. Kubetzka, and R. Wiesendanger, Science **341**, 636 (2013).
[6] A. Fert, N. Reyren, and V. Cros, Nat. Rev. Mater. **2**, 17031 (2017).
[7] S. Loth, C. P. Lutz, and A. J. Heinrich, New J. Phys. **12**, 125021 (2010).
[8] F. D. Natterer, K. Yang, W. Paul, P. Willke, T. Choi, T. Greber, A. J. Heinrich, and C. P. Lutz, Nature **543**, 226 (2017).
[9] F. D. Natterer, F. Donati, F. Patthey, and H. Brune, Phys. Rev. Lett. **121**, 027201 (2018).
[10] A. J. Heinrich, J. A. Gupta, C. P. Lutz, and D. M. Eigler, Science **306**, 466 (2004).
[11] R. M. Metzger, Chem. Rev. **115**, 5056 (2015).
[12] C. Iacovita, M. V. Rastei, B. W. Heinrich, T. Brumme, J. Kortus, L. Limot, and J. P. Bucher, Phys. Rev. Lett. **101**, 116602 (2008).
[13] V. Mourik, K. Zuo, S. M. Frolov, S. R. Plissard, E. P. A. M. Bakkers, and L. P. Kouwenhoven, Science **336**, 1003 (2012).

[14]S. Nadj-Perge, I. K. Drozdov, J. Li, H. Chen, S. Jeon, J. Seo, A. H. MacDonald, B. A. Bernevig, and A. Yazdani, Science **346**, 602 (2014).
[15]E. Y. Tsymbal, O. N. Mryasov, and P. R. LeClair, J. Phys.: Condens. Matter **15**, R109 (2003).
[16]J. S. Moodera, T. S. Santos, and T. Nagahama, J. Phys.: Condens. Matter **19**, 165202 (2007).
[17]S. Baumann, W. Paul, T. Choi, C. P. Lutz, A. Ardavan, and A. J. Heinrich, Science **350**, 417 (2015).
[18]C. L. Kane and E. J. Mele, Phys. Rev. Lett. **95**, 146802 (2005).
[19]T. Cao, F. Zhao, and S. G. Louie, Phys. Rev. Lett. **119**, 076401 (2017).
[20]M. Z. Hasan and C. L. Kane, Rev. Mod. Phys. **82**, 3045 (2010).
[21]S. Manzeli, D. Ovchinnikov, D. Pasquier, O. V. Yazyev, and A. Kis, Nat. Rev. Mater. **2**, 17033 (2017).
[22]F. Meier, L. Zhou, J. Wiebe, and R. Wiesendanger, Science **320**, 82 (2008).
[23]A. A. Khajetoorians, S. Lounis, B. Chilian, A. T. Costa, L. Zhou, D. L. Mills, J. Wiebe, and R. Wiesendanger, Phys. Rev. Lett. **106**, 037205 (2011).
[24]A. A. Khajetoorians, J. Wiebe, B. Chilian, S. Lounis, S. Blügel, and R. Wiesendanger, Nat. Phys. **8**, 497 (2012).
[25]A. A. Khajetoorians, B. Baxevanis, C. Hübner, T. Schlenk, S. Krause, T. O. Wehling, S. Lounis, A. Lichtenstein, D. Pfannkuche, J. Wiebe, and R. Wiesendanger, Science **339**, 55 (2013).
[26]R. Wiesendanger, D. Bürgler, G. Tarrach, T. Schaub, U. Hartmann, H.-J. Güntherodt, I. V. Shvets, and J. M. D. Coey, Appl. Phys. A **53**, 349 (1991).
[27]S. Rusponi, N. Weiss, T. Cren, M. Epple, and H. Brune, Appl. Phys. Lett. **87**, 162514 (2005).
[28]W. A. Hofer, K. Palotás, S. Rusponi, T. Cren, and H. Brune, Phys. Rev. Lett. **100**, 026806 (2008).
[29]S. Loth, K. von Bergmann, M. Ternes, A. F. Otte, C. P. Lutz, and A. J. Heinrich, Nat. Phys. **6**, 340 (2010).
[30]D. Huang, S. Liu, I. Zeljkovic, J. F. Mitchell, and J. E. Hoffman, Rev. Sci. Instrum. **88**, 023705 (2017).
[31]S. F. Ceballos, G. Mariotto, S. Murphy, and I. V. Shvets, Surf. Sci. **523**, 131 (2003).
[32]A. Li Bassi, C. S. Casari, D. Cattaneo, F. Donati, S. Foglio, M. Passoni, C. E. Bottani, P. Biagioni, A. Brambilla, M. Finazzi, F. Ciccacci, and L. Duò, Appl. Phys. Lett. **91**, 173120 (2007).
[33]A. Schlenhoff, S. Krause, G. Herzog, and R. Wiesendanger, Appl. Phys. Lett. **97**, 083104 (2010).
[34]S. Murphy, J. Osing, and I. V. Shvets, Appl. Surf. Sci. **144-145**, 497 (1999).
[35]H. Uchishiba, J. Phys. Soc. Jpn. **31**, 436 (1971).
[36]T. Yokoyama and K. Eguchi, Phys. Rev. Lett. **110**, 075901 (2013).
[37]T. J. Hicks, A. R. Pepper, and J. H. Smith, J. Phys. C: Solid State Phys. **1**, 1683 (1968).
[38]A. J. Melmed, J. Vac. Sci. Technol., B: Microelectron. Nanometer Struct.–Process., Meas., Phenom. **9**, 601 (1991).
[39]S. Baumann, I. G. Rau, S. Loth, C. P. Lutz, and A. J. Heinrich, ACS Nano **8**, 1739 (2014).
[40]E. Fernandes, F. Donati, F. Patthey, S. Stavrić, Ž. Šljivančanin, and H. Brune, Phys. Rev. B **96**, 045419 (2017).
[41]S. Baumann, F. Donati, S. Stepanow, S. Rusponi, W. Paul, S. Gangopadhyay, I. G. Rau, G. E. Pacchioni, L. Gragnaniello, M. Pivetta, J. Dreiser, C. Piamonteze, C. P. Lutz, R. M. Macfarlane, B. A. Jones, P. Gambardella, A. J. Heinrich, and H. Brune, Phys. Rev. Lett. **115**, 237202 (2015).
[42]K. Yang, Y. Bae, W. Paul, F. D. Natterer, P. Willke, J. L. Lado, A. Ferrón, T. Choi, J. Fernández-Rossier, A. J. Heinrich, and C. P. Lutz, Phys. Rev. Lett. **119**, 227206 (2017).
[43]W. Paul, K. Yang, S. Baumann, N. Romming, T. Choi, C. P. Lutz, and A. J. Heinrich, Nat. Phys. **13**, 403 (2017).
[44]F. Donati, S. Rusponi, S. Stepanow, C. Wäckerlin, A. Singha, L. Persichetti, R. Baltic, K. Diller, F. Patthey, E. Fernandes, J. Dreiser, Ž. Šljivančanin, K. Kummer, C. Nistor, P. Gambardella, and H. Brune, Science **352**, 318 (2016).
[45]J. S. Kasper and J. S. Kouvel, J. Phys. Chem. Solids **11**, 231 (1959).
[46]R. Gaisch, J. K. Gimzewski, B. Reihl, R. R. Schlittler, M. Tschudy, and W. D. Schneider, Ultramicroscopy **42-44**, 1621 (1992).
[47]F. D. Natterer, F. Patthey, and H. Brune, Surf. Sci. **615**, 80 (2013).

Supplementary Material for "*Antiferromagnetic MnNi tips for spin-polarized scanning probe microscopy*"

P. R. Forrester[1,2], T. Bilgeri[1], F. Patthey[1], H. Brune[1], and F. D. Natterer[1,2]

[1]Institute of Physics, École Polytechnique Fédérale de Lausanne, CH-1015 Lausanne, Switzerland
[2]Physik-Institut, University of Zurich, Winterthurerstrasse 190, CH-8057 Zurich, Switzerland

I Orientation of spin polarization for $Mn_{88}Ni_{12}$ tips

As discussed in the main text, $Mn_{88}Ni_{12}$ tips may show spin sensitivity in both the in-plane and out-of-plane directions. We do not use an in-plane sensor to quantify spin-polarization (SP) directly. Instead, we combine two observations to identify the tip as in-plane SP. The first observation is two-state switching of Ho single atom magnets (Fig. 3 of the main text), which provides information about the out-of-plane spin-polarization of the $Mn_{88}Ni_{12}$ tip. The second observation is the presence of characteristic features in *dI/dV* spectra on TiH that indicate SP in some direction [1]. In-plane sensitivity is thus inferred for tips that show the characteristic features in *dI/dV* on TiH but do not demonstrate two-state switching on holmium single atom magnets. TiH indicates SP irrespective of the orientation of the magnetic field. This is due to the prototypical spin ½ nature of this system [1,2], which does not have magneto-crystalline anisotropy. The quantization axis of TiH is consequently aligned with the magnetic field seen by the atom, which here is the stray-field of the tip. We identify a tip as SP when *dI/dV* spectroscopy on TiH shows a zero bias conductance asymmetry and large, symmetric, high energy excitations [1].

The red trace in Fig. 1(a) shows a *dI/dV* spectrum of TiH, featuring a zero bias conductance asymmetry and large, symmetric, high energy excitations. Figure 1(b) shows an $I(t)$ trace measured on a Ho single atom magnet using the same tip that recorded the SP *dI/dV*

spectrum (red) in panel (a). We observe no evidence of two-state switching on Ho using that tip, which requires out-of-plane sensitivity. Since this $Mn_{88}Ni_{12}$ tip is not sensitive to the two state switching of Ho but does demonstrate evidence of SP through the features in *dI/dV*, we conclude it is in-plane polarized.

For tips without spin sensitivity in any direction, we do not see evidence for SP on TiH. The black trace in Fig. 1(a) is a conductance spectrum of TiH measured using a non-SP $Mn_{88}Ni_{12}$ tip. Note the absence of the distinct zero bias asymmetry and the different size of the higher energy conductance steps. In agreement with *Yang et al.* [1], we identify such tips as non-SP. Accordingly, we do not see any evidence of two-state switching on Ho either.

Tips that show out-of-plane spin sensitivity many times may have nontrivial in-plane sensitivity. We recognize that using TiH and Ho as test systems does not provide insight into these cases.

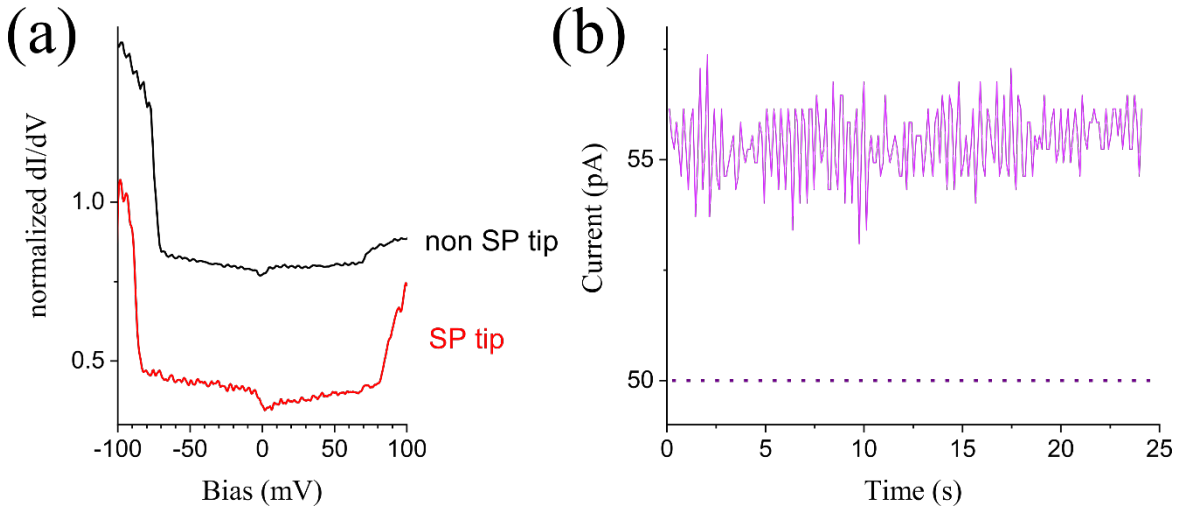

Figure 1: (a) Conductance spectra of TiH taken with a spin□polarized tip (red) (I = 200 pA, V = 100 mV, f_{mod} = 397 Hz, and V_{mod} = 2 mV_{pp}) and a non□spin□polarized tip (black) (I = 1.5 nA, V = □152 mV, f_{mod} = 397 Hz and V_{mod} = 2 mV_{pp}). The normalized spectra are offset by 0.5 units for clarity. (b) Tunneling current□time trace on Ho using the SP tip in (a) (I_{set} = 50 pA, V = □200 mV, Z□feedback off). The dotted line indicates the expected change in current that would be observed for a magnetic switching of Ho with an out-of-plane SP tip.

II Tip-originating stray field

As the SP of different microtip configurations varies, we believe the orientation of the $Mn_{88}Ni_{12}$ crystal lattice is responsible for variations in the spin-sensitivity. Although the exact structure of the tip apex is ambiguous, we provide a simple model calculation to estimate a plausible stray field for the out-of-plane and in-plane sensitive cases. We model the $Mn_{88}Ni_{12}$ crystal as a cubic lattice with a =3.67 Å and a Mn moment of 2 μ_B [3].

The upper inset in Fig. 2 shows the tip apex structure used for the out-of-plane sensitive case. Note additional layers further from the apex do not significantly contribute to the stray field due to the antiferromagnetic nature of the bulk. We assume that the tip apex is a single Mn atom and that its moment is oriented along the out-of-plane direction. The apex atom has four nearest neighbors [3]. The orientation of the moment of two of the nearest neighbors is parallel to that of the apex atom. The orientation of the moment of the other two is antiparallel. We do not include Ni atoms as their concentration is low and their contribution to the overall stray field should be minimal [3]. The red curve in Fig. 2 shows the tip-originating stray field as a function of distance in the out-of-plane direction for the geometry in the upper inset. The resulting stray field is ~14 mT in the out-of-plane direction for the tunneling conditions in Fig. 3 of the main text.

For the case of in-plane SP, we assume the single Mn apex atom has its moment oriented in-plane. The moments of the four nearest neighbors are antiparallel to that of the apex atom [Fig. 2 (lower inset)]. This reduces the effective tip-stray field to a value lower than that originating from the apex atom alone. The black trace in Fig. 2 shows the calculated stray field for this orientation. We find a stray field of ~5 mT in the in-plane direction for the tunneling conditions in Fig. 3 of the main text.

As the exact structure of the apex is unknown, different real configurations will yield different stray fields. For instance, some microtips with in-plane sensitivity may exhibit non-trivial out-of-plane stray fields and some microtips with out-of-plane sensitivity may exhibit non-trivial in-plane stray fields. The size of the stray fields is also expected to vary. Our simple calculation serves to provide a coarse estimate of the tip-originating stray field.

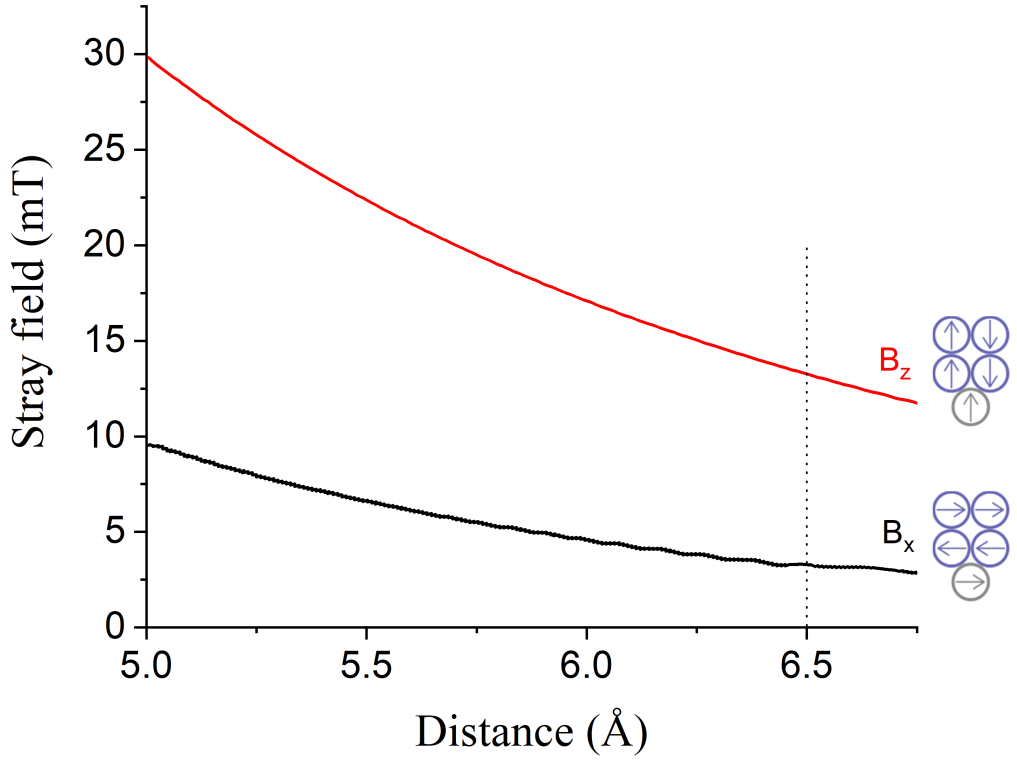

Figure 2: Tip-originating magnetic stray field as a function of distance (defined as the separation between nuclei of apex and sensor atom) for the ideal out-of-plane oriented (red) and in-plane oriented (black) geometries. Inset: schematic of tip geometries used for calculations.

III Contamination from tip etching

The tip etching procedure introduces various contaminants, which can be removed via *ex-situ* and *in-situ* cleaning. Figure 3(a) shows an SEM micrograph of an etched $Mn_{88}Ni_{12}$ tip that is not thoroughly cleaned. Figure 3(b) shows an energy dispersive X-ray analysis (EDS) spectrum of the tip in Fig. 3(a). The presence of large chlorine, carbon, and oxygen peaks suggests that the flakes are chlorine salts (from the etchant) or hydrocarbons from the solvents used to clean the tip after etching or from handling.

Figure 3(c) shows an SEM micrograph of an etched $Mn_{88}Ni_{12}$ tip after a more thorough cleaning with deionized water, acetone, and isopropanol followed by drying with pressurized nitrogen. Figure 3(e) shows an EDS spectrum of the tip in Fig. 3(c). The cleaning procedure removes most contaminants seen in Fig. 3(a-b).

Fig. 3(d, f) show an SEM micrograph and EDS spectrum, respectively, of a tip prepared as in Fig. 3(a) after argon sputtering. Sputtering leads to a smoothing of the surface roughness, fewer flakes, and an overall cleaner surface. The EDS chlorine peak after sputtering is essentially buried in noise.

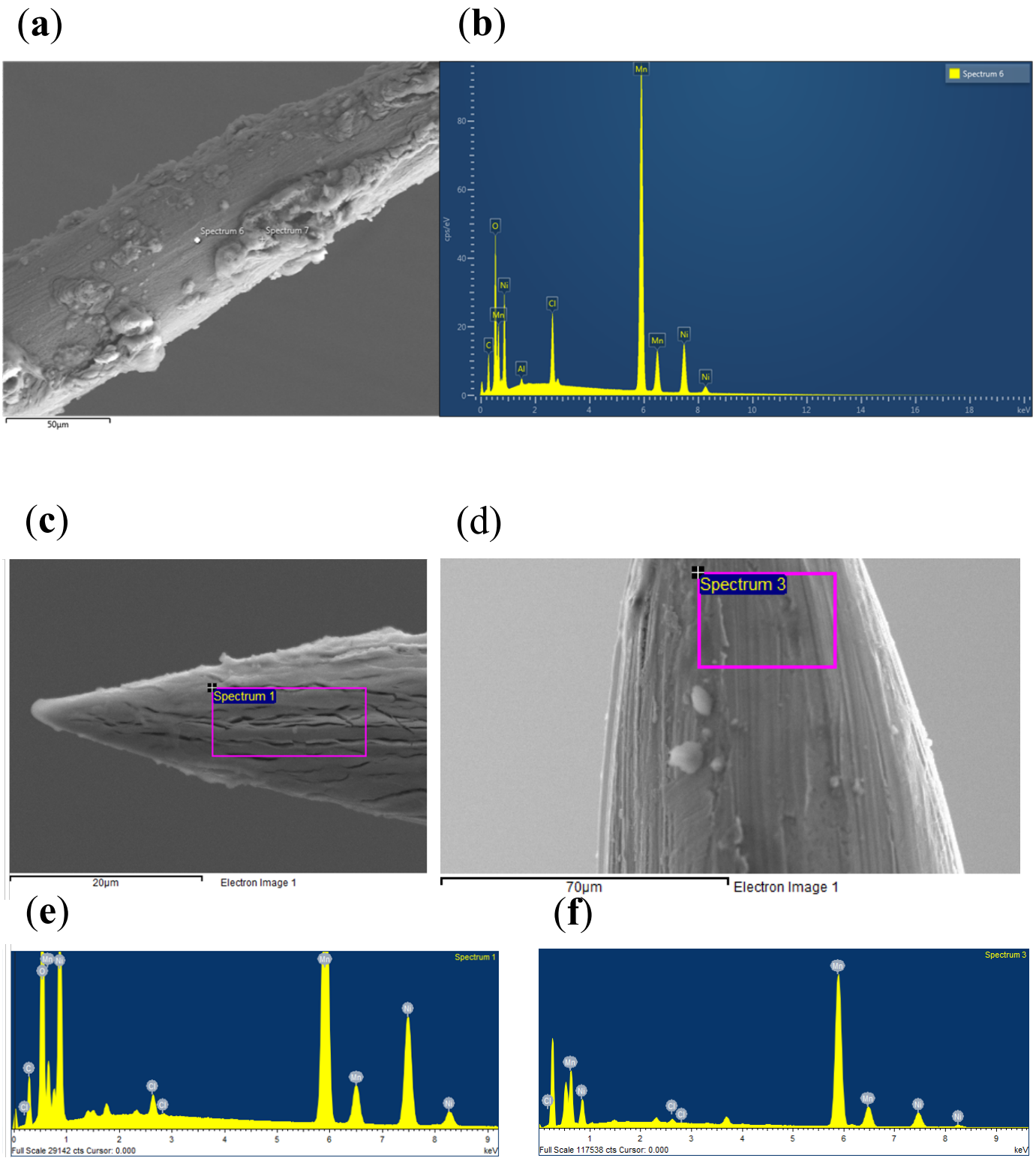

Figure 3: (a) SEM micrograph of a tip after etching without thorough cleaning. (b) EDS point spectrum [white diamond in (a)] of tip in (a). (c) SEM micrograph of a tip after etching and thorough cleaning procedure. (d) SEM micrograph of tip after etching and Ar^+ sputtering without thorough cleaning. (e) EDS spectrum of area enclosed in pink rectangle in (c). (f) EDS spectrum of area enclosed in pink rectangle in (d). All SEM micrographs imaged with a beam energy of 16 keV.

References

[1] K. Yang, Y. Bae, W. Paul, F. D. Natterer, P. Willke, J. L. Lado, A. Ferrón, T. Choi, J. Fernández-Rossier, A. J. Heinrich, and C. P. Lutz, Phys. Rev. Lett. **119**, 227206 (2017).

[2] F. D. Natterer, F. Patthey, T. Bilgeri, P. R. Forrester, N. Weiss, and H. Brune, ArXiv181003887 Cond-Mat Physics (2018).

[3] H. Uchishiba, J. Phys. Soc. Jpn. **31**, 436 (1971).